Contributed paper

OPTO-ELECTRONICS REVIEW **11**(2), 119–126 (2003)

Designing of possible structures of nitride vertical-cavity surface-emitting lasers

P. MAĆKOWIAK, T. CZYSZANOWSKI, R.P. SARZAŁA, M. WASIAK, and W. NAKWASKI*

Institute of Physics, Technical University of Łódź, 219 Wólczańska Str., 93-005 Łódź, Poland

Performance of various possible designs of 400-nm nitride vertical-cavity surface-emitting lasers (VCSELs) has been analysed with the aid of the advanced three-dimensional (3D) thermal-electrical-optical-gain self-consistent threshold simulation. It has been demonstrated that it is practically impossible to reach the fundamental-mode operation in nitride VCSELs of the traditional design with two ring contacts. To enhance this desired operation, uniformity of current injection into VCSEL active regions should be dramatically improved. Therefore we focused our research on designs with tunnel junctions and/or a semitransparent contact. In particular, it has been proved that the design with two cascading active regions, two tunnel junctions and a semitransparent contact may offer the most promising room-temperature performance characteristics for both pulse and continuous-wave operation. In particular, this design offers high mode selectivity with distinct fundamental transverse mode domination. Our simulations reveal, that the thickness and localization of a semitransparent contact as well as localization of active regions and tunnel junctions are crucial for a successful construction designing.

Keywords: computer simulation, nitride VCSEL, tunnel junction, ITO contact.

1. Introduction

Electrically pumped nitride vertical-cavity surface-emitting lasers (VCSELs) have not been reported until now at all. It is probably caused by very non-uniform carrier injection into VCSEL active regions. Uniformity of the above injection may be considerably improved with the aid of a semitransparent contact and/or tunnel junctions. A resonant-cavity nitride LED, based on such a construction, has already been demonstrated [1]. However, a VCSEL itself is still beyond the reach of this solution. According to our simulations, it is mostly due to high absorption losses associated with a semitransparent indium tin oxide (ITO) layer used in the constructions. Therefore, the main goal of this paper is to suggest the new nitride 400-nm VCSEL structure, which could overcome these difficulties. Performance characteristics of such a device are also analysed.

The structure we propose is similar to the VCSEL [2] designed years ago for the InGaAsP/InP material system, but is new in view of nitride materials. We suggest employing two cascading active regions separated by a tunnel junction to supply enough gain and to compensate losses within a semitransparent contact. Additionally, to enhance radial current flow, most of the p-type GaN layer should be replaced by n-type material and the second tunnel junction.

Performance of the proposed design of a nitride VCSEL has been analysed with the aid of an advanced 3D thermal-electrical-optical-gain self-consistent simulation. We present performance characteristics for both room-temperature (RT) pulse and RT continuous-wave (CW) operations. We also compare performance characteristics of four possible configurations of nitride VCSELs. It has been found that the proposed design enables obtaining the most promising results.

The paper is organized as follows. The model details are explained in Section 2. The structures under consideration are presented in Section 3. Simulation results are discussed in Section 4.

2. The model

The model consists of four equally important parts: optical, electrical, gain, and thermal ones. The optical model is based on the 3D optical effective frequency method [3] and takes into account realistic distributions of both parts (real and imaginary) of a complex index of refraction in all structure layers. The method enables determination of intensity profiles of all radiation modes including their gain and/or loss distributions. Lasing threshold is determined from the condition of a real propagation constant. In the optical gain calculations [4] in nitride quantum wells, the classical Fermi's golden rule, the parabolic band-gap approximation and the Lorentzian broadening mechanism are assumed.

The electrical part takes into account interplay of drift and diffusion currents of both electrons and holes. With an exception of an active region and tunnel junctions, current spreading is determined in all remaining layers from poten-

*e-mail: nakwaski@ck-sg.p.lodz.pl

Table 1. VCSEL parameters assumed in the calculations: d is the layer thicknesses (in DBR structures for both alternating layers, respectively), n_r is the refractive indices, n_g is the group refractive indices, α is the absorption coefficient ($d\alpha/dT = 0.073\ cm^{-1}/K$ is assumed for all layers), σ is the electrical conductivity, $\kappa_{300\,K}$ is the thermal conductivity at 300 K, and β_T its temperature dependence parameters [$\kappa = \kappa_{300\,K}\,(300\,K/T)^{\beta_T}$; $\kappa^{-1}_{Al_xGa_{1-x}N} = x\kappa^{-1}_{AlN} + (1-x)\,\kappa^{-1}_{GaN} + 0.05\,x\,(1-x)\ W^{-1}mK$] DBR period or QW numbers are given in brackets (Data are taken from: [a]Ref. 5, [b]Ref. 6, [c] Ref. 7, [d]Ref. 8, [e]Ref. 9, [f]Ref. 10, [g]Ref. 11, [h]Ref. 12, [i]Ref. 13, [j]Ref. 14, where not indicated, references to the data can be found in our previous publications [15–17]).

Layer		d (nm)	n_r	dn_r/dT (10^{-4}/K)	n_g	α (cm^{-1})	σ ($\Omega^{-1}\,cm^{-1}$ at 300 K/400 K)	$\kappa_{300\,K}$ ($Wm^{-1}K^{-1}$)	β_T
SiO_2 TiO_2 (4) DBR		64.1 33.3	1.56 3.00	–0.0525[e]	1.61 5.00	10	–	1.38[i] 8.9[i]	–0.31[i] 0.72[i]
TiO_2	0.899 λ		3.00	–0.0525[e]	5.00	10	–	8.9[i]	–0.72[i]
ITO		100/25	1.95	–	1.95	2000/664	2500/1850	8.2[b]	–
n-GaN spacer			2.54	2.88[f]	3.44	10	1.21/1.18	195[j]	0.264[c]
$In_{0.15}Ga_{0.85}N$ QW (5)		3.5	2.55[a]	23.2[f]	2.55[a]	2000	–	100[j]	0.264[c]
$In_{0.02}Ga_{0.98}N$ barrier (4)		3.5	2.59	2.58[f]	3.83	10	–	100[j]	0.264[c]
p-$Al_{0.2}G_{0.8}N$ blocking layer		20	2.42	0.57[g]	3.45	10	–	60	–
p-GaN		75.16	2.54	2.88[f]	3.44	10	3.82/12.7	100[j]	0.264[c]
p-InGaN:Mg++		15	2.7	23.2[f]	4.5	150	–	100[j]	0.264[c]
n-GaN:Si++		30	2.54	2.88[f]	3.44	150	–	100[j]	0.264[c]
n-GaN		64.26	2.54	2.88[f]	3.44	10	3.82/12.7	100[j]	0.264[c]
$In_{0.15}Ga_{0.85}N$ QW (5)		3.5	2.55[a]	23.2[f]	2.55[a]	2000	–	100[j]	0.264[c]
$In_{0.02}Ga_{0.98}N$ barrier (4)		3.5	2.59	2.58[f]	3.83	10	–	100[j]	0.264[c]
p-$Al_{0.2}G_{0.8}N$ blocking layer		20	2.42	0.57[g]	3.45	10	–	60	–
p-GaN		75.16	2.54	2.88[f]	3.44	10	3.82/12.7	100[j]	0.264[c]
p-InGaN:Mg++		15	2.7	23.2[f]	4.5	150	–	100[j]	0.264[c]
n-GaN:Si++		30	2.54	2.88[f]	3.44	150	–	100[j]	0.264[c]
n-GaN		80.14	2.54	2.88[f]	3.44	10	3.82/12.7	100[j]	0.264[c]
AlN $Al_{0.15}Ga_{0.85}N$ (24) DBR		47.6 40.2	2.10 2.49	0.6[h] 0.57[g]	2.67 3.53	10	–	285[d] 65	1.6[d] –
Cu heat sink		–	–	–	–	–	588200	398[i]	0.053[i]

tial distributions found by solving the Laplace equation. This 3D finite-element approach is supported by phenomenological approximation of the p-n junction current-voltage characteristics taken from the experimental results reported by Song *et al*. [1] for nitride VCSEL-like devices. Analogously, current-voltage characteristics of a tunnel junction are found for nitride devices [18,19]. We suffer from the lack of crucial parameters to accurately calculate both the above characteristics from the first principles. Therefore we have decided to use some experimental results. The model does not account for spontaneous and piezoelectric built-in fields as high carrier concentrations required to achieve lasing threshold efficiently [20] screen these fields.

Electrical conductivities are calculated using data reported by Tanaka *et al*., Yoshida *et al*., and Götz *et al*.. Further details of used approximation can be found in our previous paper [15]. The specific n-GaN contact resistance is assumed to be $3.6\times10^{-8}\ \Omega\,cm^2$ (Ti-3 nm/Au-300 nm) [16], while in the case of p-GaN we use the value of $4\times10^{-6}\ \Omega\,cm^2$ (Ni/Au 5/5 nm) [17]. The ambipolar diffusion processes in the active region are taken into account

by solving the following equation (the carrier decrease related to stimulated emission is omitted as only threshold condition is investigated here)

$$D(T)\left[\frac{\partial^2 n(r)}{\partial r^2}+\frac{1}{r}\frac{\partial n(r)}{\partial r}\right]-Cn^3(r)$$
$$-B(n,T)n^2(r)-An(r)+\frac{j(r)}{ed_A}=0 \quad (1)$$

where A is the monomolecular coefficient (10^8 s$^{-1.16}$), B is the bimolecular coefficient; its temperature dependence is evaluated based on data reported by Dmitriev *et al*. [23], while its free carrier dependence – on data reported by Smagley *et al*. [32] (0.4×10^{-10} cm^3/s at 300 K for carrier concentration of 2.1×10^{19} cm^{-3}), C is the Auger recombination coefficient (1.4×10^{-31} cm^{6}s$^{-1.16}$), D is the ambipolar diffusivity (10 cm^{2}s$^{-1.33}$ for RT), n is the free carrier concentration, j is the current density in the active region, e is the unit charge, d_A is the cumulative active region thickness, and r is the radial coordinate.

The above equation is solved using the self-consistent finite-difference method. Bimolecular [23], monomolecular and Auger recombination coefficients have been estimated as previously reported [15,34]. The first one additionally depends on excess carrier concentration [32,35], which turns out to be important at high excitation level.

The 3D finite-element thermal part of the model utilizes the same mesh as the one generated for electrical model. All calculations are performed for ambient temperature of 300 K (RT). To adequately estimate heat dissipation, we also simulate heat spreading in-5 mm thick copper heat sink. Thermal conductivity of gallium nitride has been found to strongly depend on carrier concentration [14]. Thus, for doped GaN spacers we have used distinctly lower value of thermal conductivity than in the case of nominally undoped layers of nitride DBR.

In the simulation, all the most important interactions between individual physical phenomena are taken into account including temperature and carrier concentration [36] dependencies of refractive indices and absorption, temperature- and doping-dependent thermal conductivity, electrical resistivities and optical gain. Material parameters are carefully evaluated based on recent literature values.

Table 2. Material parameters for GaN and InN: E_0 is the energy band-gap at 0 K, A_1–A_6 valence band effective-mass parameters, $m_c^{\parallel}$ is the conduction band effective mass in the k_z direction, $m_c^{\perp}$ is the conduction band effective mass in the k_x k_y plane, τ is the intraband relaxation time, b is the bowing parameter, ΔE_g is the band-gap renormalisation (Data are taken from: [a]Ref. 21, [b]Ref. 22, [c]Ref. 23, [d]Ref. 5, [e]Ref. 24, [f]Ref. 25, [g]Ref. 26,27, [h]Ref. 28, [i]Ref. 29).

	GaN	InN
E_0	3.486 eV [a,b]	1.9 eV [b]
γ	0.832×10^{-3} eV/K [a,b]	0.245×10^{-3} eV/K [c]
β	835.6 K [a,b]	624 K [c]
A_1	–6.56 [d,f]	–9.28 [d,e]
A_2	–0.91 [d,f]	–0.60 [d,e]
A_3	5.65 [d,f]	8.68 [d,e]
A_4	–2.83 [d,f]	–4.34 [d,e]
A_5	–3.13 [d,f]	–4.32 [d,e]
A_6	–4.86 [d,f]	–6.08 [d,e]
$m_c^{\parallel}$	0.20 m_0 [d,f]	0.11 m_0 [d,e]
$m_c^{\perp}$	0.18 m_0 [d,f]	0.10 m_0 [d,e]
τ	100 fs [g]	
b	1.02 [h]	
ΔE_g	-2.0×10^{-8} (n [cm^{-3}])$^{1/3}$ eV [i]	

3. The designs

Four different intracavity VCSEL designs are analysed in this paper. The desired emission wavelength for all designs is assumed to be 400 nm. To enable their comparative analysis, for all structures, 4 pairs of the dielectric SiO_2/TiO_2 distributed-Bragg reflector (DBR) are used as upper resonator mirror, 24 pairs of the semiconductor $AlN/Al_{0.15}Ga_{0.85}N$ DBR are applied on the bottom side of the structure to additionally ensure an efficient heat extraction (important in the case of the CW operation). High-reflectivity dielectric DBR mirrors have been manufactured many times for the above spectral range [18,37,38]. Recently, also analogous nitride DBR mirrors have been reported with reflectivities exceeding 99% [39,42]. More detailed analysis of the most suitable DBR configurations for nitride VCSELs can be found elsewhere [17].

The layers between the bottom and the top DBR resonator mirrors, in all structures, comprise 4-λ cavity (c.f. Fig. 1). To minimise the threshold, active regions are placed in a Fabry–Perot cavity to match gain layers with the maxima of the optical mode, and the tunnel junctions and the semitransparent contact – with its minima. In arsenide VCSELs, AlAs oxidation enables efficient lateral confinement of both carrier injection and optical field. Therefore arsenide VCSELs with active-region diameters even less than 1 μm have been reported. For nitride VCSELs, analogous method is not known. Detailed threshold analysis [17] has revealed that their optimal active regions are much larger, i.e., of a diameter equal to about 10 μm. Therefore we assume this value for all nitride VCSEL designs under consideration. Nevertheless, if an additional waveguiding mechanism is applied the diameter of the active region could be reduced to 2 μm without a significant change of the cavity optical losses. The optical confine-

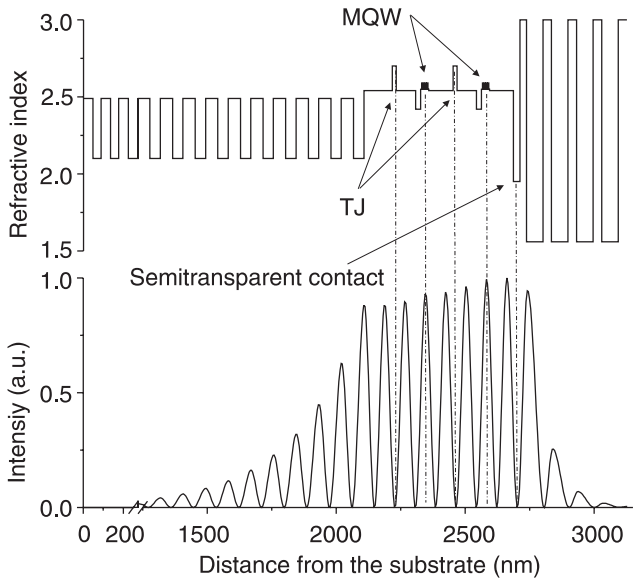

Fig. 1. Cavity design and radiation intensity distribution in the propagation direction of the modelled VCSEL with a cascade double active region (MQW), two tunnel junctions (TJs) and a semitransparent contact (C TJ ST VCSEL) for its RT CW operation.

ment of nitride VCSELs will be discussed in detail in our next paper.

The number of quantum wells is limited to 5 due to a possible interwell inhomogeneity of carrier injection [43]. For the same reason, we assume a 10% gain drop in successive wells [44]. The active region is the one analysed by Park *et al*. [45], so it is composed of the $In_{0.15}Ga_{0.85}N$ quantum well layers sandwiched by the $In_{0.02}Ga_{0.98}N$ barriers. To reduce carrier leakage, additional $Al_{0.2}Ga_{0.8}N$ blocking layers are applied.

In possible nitride VCSELs, currently available DBR mirrors (dielectric or semiconductor ones) are practically electrical isolators. Therefore the classical double lateral injection (known already in arsenide VCSELs) seems to be the most natural way to supply nitride active regions with carriers and the design with two ring contacts – its simplest realisation. Additionally, $^2H^+$ ion implantation could be used [46] to form high resistive areas between ring contacts and the lift-off technique should be employed to deposit the device on the copper heat sink [42,47]. Unfortunately, extremely non-uniform current injection takes place in the above simple VCSEL design, which enhances unwanted excitation of many high-order transverse modes and increases lasing threshold. To enhance radial current spreading improving uniformity of current injection, both tunnel junctions and semitransparent contacts may be employed. Using them, four various VCSEL designs are considered:

- NO TJ VCSEL – the above simple basic VCSEL design with two ring contacts only,
- J VCSEL – the basic design with an additional tunnel junction,
- C TJ VCSEL – the TJ VCSEL design, where an active region is replaced by a cascade double active region separated by a second tunnel junction,
- C TJ ST VCSEL – the C TJ VCSEL with an additional semitransparent contact (the whole structure of this laser design is shown in Fig. 2, while its construction parameters are listed in Tables 1, 2, and 3).

The tunnel junction used in our simulation is based on the one reported by Takeuchi *et al*. [19], so it is composed

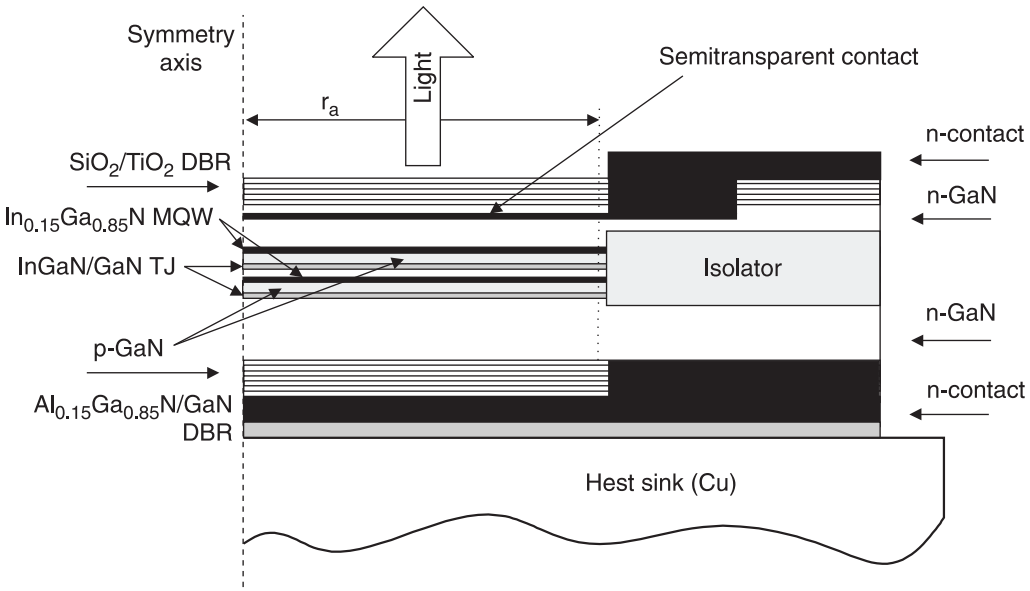

Fig. 2. The schematic structure of the modelled VCSEL with a cascade double active region (MQW), two tunnel junctions (TJs) and a semitransparent contact (C TJ ST VCSEL). The other modelled structures are variations of that design. The NO TJ VCSEL is a traditional design with one active region and intracavity ring contacts, but without tunnel junctions and a semitransparent contact. The TJ VCSEL is additionally equipped with one tunnel junction while the C TJ VCSEL is equipped with a cascade double active region and two tunnel junctions.

of 15 nm InGaN heavily doped with Mg and 30 nm GaN heavily doped with Si. The 25-nm thick semitransparent ITO contact layer is assumed with an absorption coefficient of 664 cm^{-1} and sheet resistivity of 8.6×10^{-4} $\Omega\,cm^2$ [48].

4. Results

Results of our simulation at RT are given in successive figures and in Table 3. Both CW and pulse operations are considered. To enable threshold comparison between constructions with different dominating lasing modes, we calculate for each design the modal gains for various modes. The results for fundamental LP_{01} modes (lines 4 and 15) and for dominating modes (lines 5 and 16) of each structure are listed in Table 3. For all constructions under consideration, the driving voltage is chosen to be only somewhat above the threshold lasing condition.

The traditional VCSEL structure (NO TJ VCSEL) exhibits a very strong current crowding effect near the active-region edge, whereas nearly insignificant current density is injected into the central part of its active region [Fig. 3(a)]. This causes highly non-uniform carrier concentration distribution [Fig. 3(b)], very high close to the active-region perimeter (Table 3: lines 10 and 19) and much lower in the centre (lines 11 and 20). Subsequently, material gain

Table 3. Selected results of the simulations of room-temperature threshold operation for four analysed structures, see text for descriptions of abbreviations, U, I is the driving voltage and current, respectively, and λ is the wavelength of emitted radiation.

No.	Parameter	NO TJ VCSEL	TJ VCSEL	C TJ VCSEL	C TJ ST VCSEL
1	U_{th}, V	7	7	13	13
	Continuous wave operation				
2	I_{th}, mA	11.8	15.6	10.0	11.6
3	λ, nm	~401	~401	~402	~405
4	Modal gain of the LP_{01}mode, cm^{-1}	+12.9	+13.7	+63.4	+80.3
5	Highest modal gain /mode, cm^{-1}	+16.2 $LP_{8\,1}$	+13.9 $LP_{2\,1}$	+64.1 $LP_{3\,1}$	+80.3 $LP_{0\,1}$
6	Highest optical gain in active region, cm^{-1}	7945	6507	5547	6257
7	Lowest optical gain in active region, cm^{-1}	2582	6061	5185	4492
8	Highest temperature in active region, K	328	332	348	353
9	Lowest temperature in active region, K	317	322	332	331
10	Highest carrier concentration in active region, 10^{19} cm^{-3}	5.7	4.6	4.2	4.8
11	Lowest carrier concentration in active region, 10^{19} cm^{-3}	2.0	3.6	3.2	2.7
12	Highest current density, kA/cm^2	106	61	50	14
	Pulse operation				
13	I_{th}, mA	8.8	12.2	9.8	10.3
14	λ, nm	~400	~400	~400	~400
15	Modal gain of the LP_{01}mode, cm^{-1}	-6.42	+12.5	+77.2	+87.4
16	Highest modal gain /mode, cm^{-1}	−6.38 $LP_{1\,1}$	+12.5 $LP_{0\,1}$	+77.2 $LP_{0\,1}$	+87.4 $LP_{0\,1}$
17	Highest optical gain in active region, cm^{-1}	6822	6847	6215	6854
18	Lowest optical gain in active region, cm^{-1}	2193	6263	5589	4852
19	Highest carrier concentration in active region, 10^{19} cm^{-3}	4.5	4.4	3.9	4.4
20	Lowest carrier concentration in active region, 10^{19} cm^{-3}	1.8	3.4	3.0	2.5
21	Highest current density, kA/cm^2	76	58	47	14

non-uniformity (lines 6,7 and 17,18) strongly favours unwanted higher-order transverse modes [see Fig. 3(c)].

Uniformity of current injection is considerably improved in the TJ VCSEL. By introducing a tunnel junction in the cavity, one can almost completely replace low electrically conductive p-type GaN spacer by its *n*-type counterpart. In this way overall series resistance of the device can be reduced and, more importantly, radial current flow is significantly enhanced. Therefore the dominant excitation of the fundamental LP_{01} mode in the case of RT pulse operation may be expected. For the RT CW operation, however, the dominating mode is LP_{21}, which once again confirms the importance of the radial temperature distribution in nitride VCSELs [Fig. 3(d)].

The third design (C TJ VCSEL) is additionally equipped with the cascade double active region. It results in much higher optical gain (achieved for lower current – Table 3: line 2) in comparison with NO TJ and TJ VCSELs (c.f. Table 3: lines 5 and 16). It may be especially important for RT CW operated nitride VCSELs, where the active region temperature at threshold is relatively high [c.f. Fig. 3(d)] which is followed by a significant reduction of optical gain. The dominating mode for this operation is still a non-fundamental mode, however, the differences in the average absorption losses between low order transverse modes are nearly insignificant. Thus, one may expect a multimode operation with mode switching for that design during its RT CW operation. On the other hand, a single-fundamental mode-operation is likely to occur for the RT pulse operation.

The fourth design (C TJ ST VCSEL) is based on the third one. An additional semitransparent contact drastically reduces the peak of current density near the active region perimeter [cf. Fig. 3(a)] and the current injection becomes nearly ideally uniform. However, the contact introduces additional optical absorption, therefore it should be thin enough and its position should fit the node of the resonator standing wave. Surprisingly, the threshold RT CW driving current for the C TJ ST VCSEL is only slightly higher than that for the C TJ VCSEL (c.f. Table 3: lines 2), while the modal gain is much higher for the former design (by more than 25%, c.f. Table 3: lines 5 and 16). Such a significant difference can be explained by a strong index guiding effect caused by more appropriate radial temperature profile

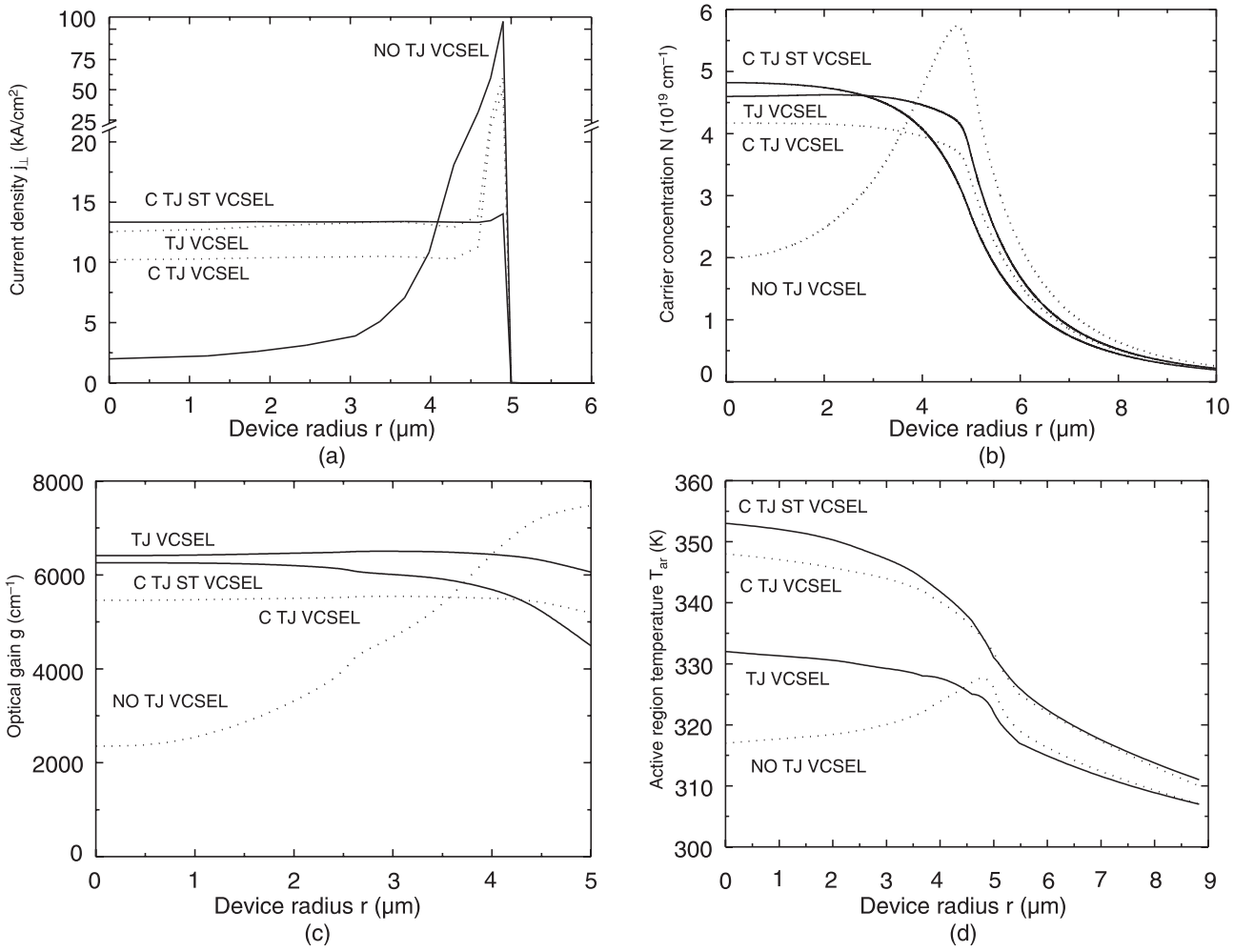

Fig. 3. Radial distribution of the active region current density (a), carrier concentration (b), optical gain (c), and temperature (d) for the modelled nitride VCSELs and their RT CW operation (see the caption of Fig. 2 and the text for the notation used).

[Fig. 3(d)]. Therefore, the optical mode could be better confined and the overlapping between mode intensity and gain distribution may be higher. As a consequence, the fundamental transverse mode of the C TJ ST VCSEL is excited first for both the RT pulse and the RT CW operations. According to our simulation, the lasing condition could be achieved at the average current density around 10 kAcm^{-2}. It should be, however, remembered that we considered nearly ideal thin semitransparent material [48] (c.f. Table 1). Nevertheless, the use of a semitransparent contact with conjunction with a cascade double active region may be expected to be a very promising design.

5. Conclusions

We have used an advanced 3D thermal-optical-electrical-gain self-consistent model to compare usability of various designs and to construct first electrically pumped RT CW 400-nm nitride VCSELs. It has been found that for the fundamental-mode operation, current injection into a VCSEL active region should be at least uniform if not of a bell-like shape. We focused our research on designs with tunnel junctions and a semitransparent contact, which are known to improve the above uniformity.

The results suggest that the best performance may be expected in the C TJ ST VCSEL with two cascading active regions, two tunnel junctions and a thin semitransparent contact. In particular, the semitransparent contact has been found to considerably enhance the uniformity of current injection but it may introduce huge optical absorption losses. Therefore its thickness and an appropriate localisation in the node of a resonator standing wave is crucial for a successful construction. Besides, both active regions should be placed in maxima positions of the resonator standing wave (to supply enough gain to compensate additional losses associated with a semitransparent contact), whereas both tunnel junctions – in its node positions (c.f. Fig. 1). High optical gain is especially important for nitride VCSELs, where the active-region temperature at threshold is relatively high and the following reduction of optical gain is significant.

It has been found that the design we propose enables obtaining the most promising results for both the RT CW and the RT pulse operations. The semitransparent contact significantly enhances uniformity of a current injection into the active region and considerably reduces the peak of current density near the active region perimeter. The radial temperature profile for that design enhances an additional thermal waveguiding effect, which in turn reduces the CW threshold and results in the domination of the fundamental transverse LP_{01} mode for the RT CW operation. During the RT pulse operation, the LP_{01} mode also exhibits the lowest threshold and, more surprisingly, the structure achieves higher mode selectivity.

The present threshold analysis does not take into account a negative feedback between the intensity standing wave and the carrier concentration distribution, known as the spatial hole-burning (SHB) effect. With an increase in an operation current over its threshold value, the SHB effect causes a gradual reduction of the gain of a dominating mode leading finally to an excitation of another one. Therefore, to enhance the single-mode-operation (preferably – fundamental-mode-operation), it is not enough to obtain a uniform current injection – material gain profile should be as similar as possible to the intensity profile of a chosen mode.

Acknowledgements

This work was supported by the Polish State Committee for Scientific Research (KBN), grants No 7T11B06920 and No 7T11B07321.

References

1. Y.K. Song, M. Diagne, H. Zhou, A.V. Nurmikko, R.P. Schneider Jr, and T. Takeuchi, "Resonant-cavity InGaN quantum-well blue light-emitting diodes", *Appl. Phys. Lett.* **77**, 1744–1746 (2000).
2. S. Uchiyama and K. Iga, "Consideration on threshold current density of GaInAsP/InP surface emitting junction lasers", *IEEE J. Quantum Electron.* **QE-22**, 302–309 (1986).
3. H. Wenzel and H.J. Wünsche, "The effective frequency method in the analysis of vertical-cavity surface-emitting lasers", *IEEE J. Quantum Electron.* **33**, 1156–1162 (1997).
4. S.L. Chuang, *Physics of Optoelectronic Devices,* Chapter 10.3, Wiley, New York, 1995.
5. M. Mandy. Y. Leung, A.B. Djurisic, and E.H. Li, "Refractive index of InGaN/GaN quantum well", *J. Appl. Phys.* **84**, 6312–6317 (1998).
6. S.M.D. Tosoh: Product Data Sheets (www.tosohsmd.com).
7. E.K. Sichel and J.I Pankove, "Thermal conductivity of GaN, 25–360 K", *J. Phys. Chem. Solids* **38**, 30 (1977).
8. G.A. Slack, R.A. Tanzil, R.O. Pohl, and J.W. Vandersande, "The intrinsic thermal conductivity of AlN", *J. Phys. Chem. Solids* **48**, 641–647 (1987).
9. Landolt-Börnstein, *Numerical Data and Functional Relationships in Science and Technology*, Springer, Berlin, 1962.
10. G.Y. Zhao, H. Ishikawa, G. Yu, T. Egawa, J. Watanabe, T. Soga, T. Jimbo, and M. Umeno, "Thermo-optical nonlinearity of GaN grown by metalorganic chemical-vapour deposition", *Appl. Phys. Lett.* **73**, 22-24 (1998).
12. X. Tang, Y. Yuan, K. Wonchotigul, M.G. Spencer, H. Ying, and Z. Ling, "Study of thermo-optic properties of aluminium nitride waveguides", *Proc. SPIE* **3283**, 938–941 (1998).
13. Y.S. Toulokian, R.W. Powell, C.Y. Ho, and P.G. Klemens, *Thermophysical Properties of Matter* **1-2**, IFI/Plenum, New York, 1970.
14. D.I. Florescu, V.A. Asnin, L.G. Mourokh, F.H. Pollak, R.J. Molnar, and C.E.C. Wood, "High spatial resolution thermal conductivity and Raman spectroscopy investigation of hydride vapour phase epitaxy grown n-GaN/sapphire (0001): Doping dependence", *J. Appl. Phys.* **88**, 3295–3300 (2000).
15. P. Maćkowiak and W. Nakwaski, "Detailed threshold analysis of UV-emitting nitride vertical-cavity surface-emitting lasers", *J. Physics D: Appl. Physics* **31**, 2479-2484 (1998).

16. P. Maćkowiak and W. Nakwaski, "Designing guidelines for possible continuous-wave-operating nitride vertical-cavity surface-emitting lasers", *J. Physics D: Applied Physics* **33**, 642–653 (2000).
17. P. Maćkowiak and W. Nakwaski, "Some aspects of designing an efficient nitride VCSEL resonator", *J. Physics D: Applied Physics* **34**, 954–958 (2001).
18. S.R. Jeon, Y.H. Song, H.J. Jang, G.M. Yang, S.W. Hwang, and S J. Son, "Lateral spreading in GaN-based light-emitting diodes utilising tunnel contact junctions", *Appl. Phys. Lett.* **78**, 3265–3267 (2001).
19. T. Takeuchi, G. Hasnain, S. Corzine, M. Huechen, R.P. Schneider, Jr., Ch. Kocot, M. Blomqvist, Y. Chang, D. Lefforge, M.R. Krames, L.W. Cook, and S.A. Stockman, "GaN-based light emitting diodes with tunnel junction", *Jpn. J. Appl. Phys.* **40**, L861–L863 (2001).
20. F. Della Sala, A. Di Carlo, and P. Lugli, F. Bernardini, V. Fiorentini, R. Scholz, and J.M. Jancu, "Free-carrier screening of polarization fields in wurtzite GaN/InGaN laser structures", *Appl. Phys. Lett.* **74**, 2002–2004 (1999).
21. W. Shan, T.J. Schmidt, X.H. Yang, S.J. Hwang, and J.J. Song, "Temperature dependence of interband transitions in GaN grown by metalorganic chemical vapour deposition", *Appl. Phys. Lett.* **66**, 985–987 (1995).
22. H. Jiang and J. Singh, "Gain characteristics of InGaN-GaN quantum wells", *IEEE J. Quantum Electron.* **36**, 1058–1064 (2000).
23. A. Dmitriev and A. Oruzheinikov, "The rate of radiative recombination in nitride semiconductors and alloys", *J. Appl. Phys.* **86**, 3241–3245 (1999).
24. Y.C. Yeo, T.C. Chong, and M F. Li, "Electronic band structures and effective-mass parameters of wurtzite GaN and InN", *J. Appl. Phys.* **83**, 1429–1436 (1998).
25. M. Suzuki and T. Uenoyama, "First-principles calculations of effective-mass parameters of AlN and GaN", *Phys. Rev.* **B52**, 8132–8139 (1995).
26. Y.C. Yeo, T.C. Chong, M.F. Li, and W.J. Fan, "Analysis of optical gain and threshold current density of wurtzite InGaN/GaN/AlGaN quantum well lasers", *J. Appl. Phys.* **84**, 1813–1819 (1998).
27. A.T. Meney, E.P. O'Reilly, and A.R. Adams, "Optical gain in wide bandgap GaN quantum well lasers", *Semicond. Sci. Technol.* **11**, 897–903 (1996).
28. A.F. Wright and J.S. Nelson, "Bowing parameters for zinc-blende $Al_{1-x}Ga_xN$ and $Ga_{1-x}In_xN$, *Appl. Phys. Lett.* **66**, 3051–3053 (1995).
29. A. Zukauskas, S. Juresenas, G. Kurilcik, G. Tamulaitis, M.S. Shur, R. Gaska, J.W. Yang, and M.A. Khan, "Finite-temperature, band gap renormalisation in highly photoexcited GaN epilayers", *Phys. Stat. Sol. (b)* **216**, 501–504 (1999).
30. J. Burm, K. Chu, W.A. Davis, W.J. Schaff, and L.F. Eastman, "Ultra-low resistive ohmic contacts on n-GaN using Si implantation", *Appl. Phys. Lett.* **70**, 464–466 (1997).
31. L.Ch. Chen, J.K. Ho, Ch.Sh. Jong, Ch.C. Chiu, K.K Shih, F.R Chen, J.J Kai, and L. Chang, "Oxidized Ni/Pt and Ni/Au ohmic contacts to p-type GaN", *Appl. Phys. Lett.* **76**, 3703–3705 (2000).
32. V.A. Smagley, P.G. Eliseev, and M. Osiński, "Comparison of models for optical gain in gallium nitride", *Proc. SPIE* **2994**, 129–140 (1997).
33. A. Vertikov, I. Ozden, and A.V. Nurmikko, "Diffusion and relaxation of excess carriers in InGaN quantum wells in localised versus extended states", *J. Appl. Phys.* **86**, 4697-4699 (1999).
34. P. Maćkowiak and W. Nakwaski, "Threshold currents of nitride vertical-cavity surface-emitting lasers with various active regions", *MRS Internet J. Nitride Semicond. Research* **3**, Article 35, 1998.
35. S.H. Park, S.L. Chuang, and D. Ahn, "Piezoelectric effects on many-body optical gain of zinc-blende and wurtzite GaN/AlGaN quantum-well lasers", *Appl. Phys. Lett.* **75**, 1354–1356 (1999).
36. H.X. Jiang and J.Y. Lin, "Mode spacing 'anomaly' in InGaN blue lasers", *Appl. Phys. Lett.* **74**, 1066–1068 (1999).
37. T. Someya, K. Tachibana, J. Lee, T. Kamiya, and Y. Arakawa, "Lasing emission from $In_{0.1}Ga_{0.9}N$ vertical cavity surface emitting laser", *Jpn. J. Appl. Phys.* **37**, L1424–L1426 (1998).
38. Y.K. Song, H. Zhou, M. Diagne, A.V. Nurmikko, R.P. Schneider Jr., C.P. Kuo, M.R. Krames, R.S. Kern, C. Carter-Coman, and F.A. Kish, "A quasicontinuous wave, optically pumped violet vertical cavity surface emitting laser", *Appl. Phys. Lett.* **76**, 1662–1664 (2000).
39. K.E. Waldrip, J. Han, J.J. Figel, H. Zhou, E. Makarona, and A.V. Nurmikko, "Stress engineering during metalorganic chemical vapour deposition of AlGaN/GaN distributed Bragg reflectors", *Appl. Phys. Lett.* **78**, 3205–3207 (2001).
40. T.T. Someya, R. Werner, A. Forchel, M. Catalano, R. Cingolani, and Y. Arakawa, "Room temperature lasing at blue wavelengths in gallium nitride microcavities", *Science* **285**, 1905–1906 (1999).
41. H.M. Ng, D. Doppalapudi, D.E. Iliopouls, and T.D. Moustakas, "Distributed Bragg reflectors based on Aln/GaN multilayers", *Appl. Phys. Lett.* **74**, 1036–1038 (1999).
42. Y.K. Song, M. Diagne, H. Zhou, A.V. Nurmikko, C. Carter-Coman, R.S. Kern, F.A. Kish, and M.R. Kramers, "A vertical injection blue light emitting diode in substrate separated InGaN heterostructures", *Appl. Phys. Lett.* **74**, 3720–3722 (1999).
43. K. Domen, R. Soejima, A. Kuramata, K. Horino, S. Kubota, and T. Tanahashi, "Interwell inhomogeneity of carrier injection in InGaN/GaN/AlGaN multiquantum well lasers", *Appl. Phys. Lett.* **73**, 2775–2777 (1998).
44. N. Tessler and G. Eisenstein, "On carrier injection and gain dynamics in quantum well lasers", *IEEE J. Quantum Electron.* **29**, 1586–1595 (1993).
45. S.H. Park and S.L. Chuang, "Many-body optical gain of wurtzite Gan-based quantum-well lasers and comparision with experiment", *Appl. Phys. Lett.* **72**, 287–289 (1998).
46. S.J. Pearton, R.G. Wilson, J.M. Zavada, J. Han, and R.J. Shul, "Thermal stability of ^{2}H-implanted n- and p-type GaN", *Appl. Phys. Lett.* **73**, 1877–1879 (1998).
47. W.S. Wong, M. Kneissel, P. Mei, D.W. Treat, M. Teepe, and N.M. Johnson, "The integration of $In_xGa_{1-x}N$ multiple-quantum-well laser diodes with copper substrate by laser lift-off", *Jpn. J. Appl. Phys.* **39**, L1203–L1205 (2000).
48. T. Margalith, O. Buchinsky, D.A. Cohen, A.C. Abare, M. Hansen, S.P. DenBaars, and L.A. Coldren "Indium tin oxide contacts to gallium nitride optoelectronic devices", *Appl. Phys. Lett.* **74**, 3930–3932 (1999).

